Revisiting the growth mechanism of atomic layer deposition of Al2O3

Revisiting the growth mechanism of atomic layer deposition of Al_2O_3: A vibrational sum-frequency generation study

Vincent Vandalon, and W. M. M. (Erwin) Kessels

Citation: Journal of Vacuum Science & Technology A: Vacuum, Surfaces, and Films **35**, 05C313 (2017); doi: 10.1116/1.4993597

View online: http://dx.doi.org/10.1116/1.4993597

View Table of Contents: http://avs.scitation.org/toc/jva/35/5

Published by the American Vacuum Society

Revisiting the growth mechanism of atomic layer deposition of Al_2O_3: A vibrational sum-frequency generation study

Vincent Vandalon[a] and W. M. M. (Erwin) Kessels
Department of Applied Physics, Eindhoven University of Technology, P.O. Box 513, 5600 MB Eindhoven, The Netherlands

(Received 11 May 2017; accepted 28 June 2017; published 21 July 2017)

The growth mechanism of the prototypical atomic layer deposition (ALD) process of Al_2O_3 using $Al(CH_3)_3$ (TMA) and H_2O has been revisited on the basis of insights obtained with the nonlinear optical analysis technique of broadband sum-frequency generation (BB-SFG). With BB-SFG spectroscopy, both the $–CH_3$ and –OH surface groups ruling the growth of Al_2O_3 by ALD were detected and could be monitored during the ALD process with submonolayer sensitivity. Several remaining questions pertaining to the growth mechanism of Al_2O_3 were addressed. The reaction kinetics of the H_2O half-cycle were studied for ALD between 100 and 300 °C, and the reaction cross section σ was determined. The cross section at 300 °C was fairly large ($\sigma = 3 \times 10^{-19}$ cm^2) and it decreased with decreasing temperature. Below 200 °C, the cross section also clearly varied with the surface coverage. For example, at 100 °C, the cross section started at $\sigma = 1 \times 10^{-20}$ cm^2 for a full $–CH_3$ coverage and decreased to $\sigma = 3 \times 10^{-21}$ cm^2 for a 60% coverage. This coverage dependence of the reaction kinetics also explains the presence of the *persistent* $–CH_3$ groups at low temperatures which are no longer reactive toward H_2O. By a dedicated study using x-ray photo-emission spectroscopy, it was demonstrated that the *persistent* $–CH_3$ groups were not incorporated into the film as a contaminant species. The absolute $–CH_3$ coverage was measured for ALD between 100 and 450 °C. With this data, steric hindrance was ruled out as the cause of the self-limiting behavior in the TMA half-cycle on basis of the decrease observed in the $–CH_3$ coverage with temperature. The self-limiting behavior was attributed to the depletion of under coordinated O during the TMA half-cycle. Moreover, the chemisorption of TMA on the -OH surface groups during the TMA half-cycle was investigated. On average, 1.5 $–CH_3$ ligands remained on the surface per deposited Al atom after the TMA half-cycle at 300 °C, and this number decreased to 0.8 at 100 °C. These insights into the underlying growth mechanism augment the understanding of Al_2O_3 ALD and reveal several nuances in this well-studied ALD process. © *2017 American Vacuum Society*.
[http://dx.doi.org/10.1116/1.4993597]

I. INTRODUCTION

In microelectronics and related fields, many key advances in dry etching and thin-film deposition have been the result of detailed insight into the underlying fundamental surface reactions. The pioneering work by Coburn and Winters has been exemplary for the approach used in mechanistic studies in semiconductor processing by etching and deposition.[1] They introduced a methodology combining the systematic aspects of fundamental surface-science studies with the close-to-actual operation conditions and the nonideal surfaces used in the etch processes.[1–4] On these nonideal surfaces, additional processes can occur that are critical for understanding the etching mechanism. The value of this approach was demonstrated by their seminal work on Si etching.[1–4] Similar processes play a role in the growth of thin-films by methods such as atomic layer deposition (ALD).

ALD is an enabling technology for the fabrication of semiconductor devices because of its capability to uniformly and conformally cover complex 3D structures with thin films with subnanometer thickness control.[5] The capabilities of ALD processes are inherent to their underlying growth mechanism.[5] In essence, ALD consists of a sequence of self-limiting surface reactions which together deposit an "atomic layer" of material.[5] The repeatable sequence of steps is called an ALD cycle and the number of cycles can be chosen to grow a film with a certain thickness.

Currently, there is a push toward even more demanding applications for ALD films. A good example of this trend is the deposition of ALD films on temperature sensitive substrates requiring the development of low temperature or even room temperature ALD processes.[6–8] In order to meet these evermore demanding requirements in a systematic way, it is essential to gain a better understanding of the surface reactions governing the ALD process. This calls for an approach similar to that of Coburn and Winters, and the success of earlier mechanistic studies of ALD growth processes highlights the value of this approach.[6,9,10]

This work focuses on the surface chemistry of the prototypical ALD process growing Al_2O_3 using trimethylaluminum [TMA, $Al(CH_3)_3$] as precursor and water as coreactant. This process serves as a model system for ALD of metal-oxides with metal-organic precursors. Moreover, it is one of the more ubiquitous ALD processes.[6,9–15] Higashi and Fleming introduced the ALD process of Al_2O_3 and they reported on its key aspects as well as noteworthy properties

[a]Electronic mail: v.vandalon@tue.nl

of the resulting Al_2O_3 films.[11] Ensuing, many details of this ALD process have been studied intensively, and as a result, the growth mechanism is fairly well understood as will be addressed in Sec. II.[9,12,13,16,17] Nevertheless, new insights into some of the fundamental mechanisms of this ALD process can be gained. For example, in our previous work we reported on the fundamental mechanism causing the commonly observed decrease in growth-per-cycle (GPC) at low temperatures. It was demonstrated that this decrease in GPC was caused by *persistent* $–CH_3$ groups present on the surface at low temperatures.[18] Basically, these *persistent* $–CH_3$ groups limit the TMA uptake and therefore result in a lower GPC. Ensuing, it was demonstrated by others that these *persistent* groups play a key role in other ALD processes as well.[19]

For the Al_2O_3 ALD process, several open questions pertaining to the growth mechanism were identified and investigated here: First, the origin of the self-limiting behavior in the precursor half-cycle is still debated in the literature.[13,14,20] The conclusions drawn from experiments have been contradictory,[13,14] and recently, this topic has been studied using density functional theory (DFT) indicating the need for further experimental work.[20] Second, how the TMA chemisorbs on the -OH terminated surface is of interest. So far, indirect measurements by quadrupole mass spectrometry (QMS) and quartz-crystal microbalance have shed some light on this topic; however, a more direct measurement is desirable.[16] Third, in our previous work, the temperature dependence of the reaction kinetics was found to be relatively complex, and it was concluded that they should be studied in more detail.[18] Finally, the apparent paradox between virtually carbon free Al_2O_3 films, as typically reported for ALD,[21] and the presence of the *persistent* $–CH_3$ groups at low temperatures needs to be addressed.

The nonlinear optical technique of broadband sum-frequency generation (BB-SFG) was used to study the surface chemistry during ALD of Al_2O_3. BB-SFG spectroscopy is a state of the art technique, predominantly used in the field of surface science, which is now utilized to study the surface chemistry of ALD in this work. BB-SFG spectroscopy is ideally suited for this task because of its submonolayer sensitivity, inherent surface selectivity, and fairly short acquisition times. In short, the BB-SFG signal is generated by simultaneously exposing the surface groups to a picosecond visible pulse and a femtosecond broadband mid-IR pulse.[22,23] These two pulses mix, generating a new signal in the visible part of the spectrum. The mixing is resonantly enhanced for photon energies matching a vibrational transition of the surface groups.[22] As a result, a part of the vibrational fingerprint of the surface groups is present in the visible BB-SFG signal. The surface groups can be identified by the unique spectral position of the resonances, and the density of the surface groups is proportional to the strength of those resonant signals. For example, the C-H stretch mode of $–CH_3$ groups at $\sim 2900\,cm^{-1}$ can be used to identify the presence of these groups and to study their density on the surface. A key merit of BB-SFG spectroscopy is that the detected signals are proportional to the square of the absolute surface coverage. Moreover, because of its inherent surface selectivity, differential spectra are not required. This allows a more direct interpretation of the data and requires less prior knowledge of the system under investigation than a differential technique such as Fourier transform IR (FTIR) absorption spectroscopy.

Because BB-SFG spectroscopy is not yet established in the field of ALD, it is valuable to explore its capabilities and verify whether the $–CH_3$ and –OH surface groups resulting from TMA and H_2O exposure during ALD can be detected. For this purpose, an isotope study using H_2O, D_2O, $Al(CH_3)_3$, and $Al(CD_3)_3$ was performed. The aforementioned open questions were investigated with BB-SFG spectroscopy. The reaction kinetics during the H_2O half-cycle was studied by BB-SFG spectroscopy by measuring the $–CH_3$ density as a function of coreactant exposure, i.e., a type of saturation curve was established. To address the influence of temperature on the reaction kinetics, these experiments were performed at different temperatures ranging from 100 up to 300 °C. To gain more quantitative information about the surface chemistry, the absolute areal density of $–CH_3$ surface groups was determined after both half-cycles for ALD between 100 and 450 °C. This data yielded insights into the origin of the self-limiting nature of the ALD reactions and the chemisorption of TMA itself. A separate x-ray photo-emission spectroscopy (XPS) experiment was performed to study the possible incorporation of carbon into the film from $–CH_3$ groups remaining at the surface after the H_2O step.

The manuscript is organized as follows: A brief recapitulation of the growth mechanism of Al_2O_3 ALD is given in Sec. II. This provides the necessary background for the interpretation of the experimental results and puts the results in their proper perspective. In Sec. III, the experimental details are given. In Sec. IV, the results are presented and discussed. The section is divided into four parts: basic surface chemistry, reaction kinetics, quantification of the $–CH_3$ coverage, and carbon incorporation. In Sec. V, the main conclusions are given.

II. GROWTH MECHANISM OF ALD OF Al_2O_3

The growth of Al_2O_3 during steady-state ALD is ruled by surface chemistry involving predominantly $–CH_3$ and –OH groups. A schematic representation of the growth mechanism is shown in Fig. 1. At the beginning of the TMA half-cycle, the surface is –OH terminated. This surface is exposed to vapor phase TMA which chemisorbs on the -OH groups. Each chemisorbed TMA molecule reacts with one or two –OH groups. This ligand exchange reaction releases gas phase CH_4 as a volatile reaction product. After a sufficiently large precursor exposure, no more TMA can chemisorb on the surface. This is the self-limiting aspect of the chemistry, and the half-cycle is said to be "in saturation," resulting in a $–CH_3$ terminated surface. At the end of the TMA half-cycle, the gas phase reaction products (CH_4) and excess precursor are removed from the reactor by purging and/or pumping. In the ensuing H_2O half-cycle, vapor phase H_2O reacts with the

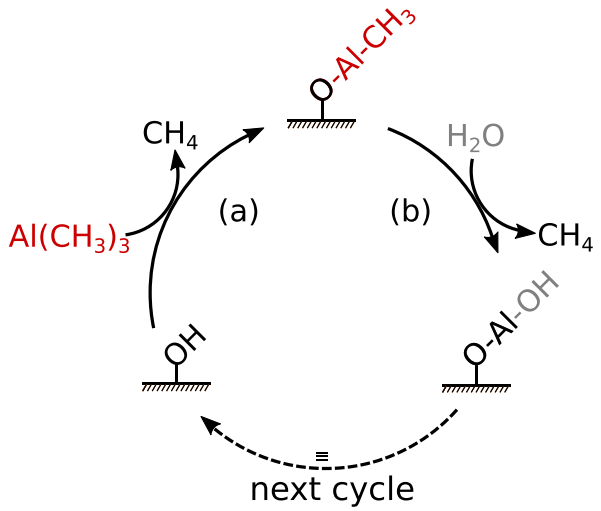

FIG. 1. (Color online) The cyclical ALD process for Al_2O_3 can be divided into a TMA and a H_2O half-cycle. (a) In the TMA half-cycle, vapor phase TMA reacts with the –OH groups on the surface depositing a submonolayer of Al atoms terminated by $–CH_3$ groups. (b) In the ensuing H_2O half-cycle, water vapor reacts with the $–CH_3$ groups converting the surface layer into Al_2O_3 and recuperating a –OH terminated surface. Gas phase CH_4 is released in both the TMA and the H_2O half-cycle as a reaction product that is removed from the reactor by pumping and/or purging before the next ALD half-cycle.

$–CH_3$ groups on the surface. This ligand exchange reaction replaces the $–CH_3$ groups with –OH groups and again releases gas phase CH_4. This reaction is also self-limiting, and at the end of this half-cycle, the remaining coreactant molecules and gas phase reaction products are again removed by purging and/or pumping. The surface is now –OH terminated while a layer of Al_2O_3 has been deposited, and the cycle can be repeated. In their simplest form, these reactions can be summarized as follows:

$$x-\mathrm{OH}+\mathrm{Al(CH_3)_3}\rightarrow-\mathrm{OAl(CH_3)}_x+(3-x)\mathrm{CH_4}, \quad (1a)$$

$$-\mathrm{Al(CH_3)}+\mathrm{H_2O}\rightarrow-\mathrm{AlOH}+\mathrm{CH_4}. \quad (1b)$$

In these equations, the "–" sign indicates a surface species and x represents the number of $–CH_3$ ligands bonded to Al remaining after chemisorption. There exist several secondary reaction pathways with, e.g., different reactive sites that might contribute to the ALD growth. For example, TMA chemisorption has been shown to occur on Al–O–Al bridges,[14] carbonates,[24,25] and formates.[26] However, the growth via these secondary reaction paths is generally small compared to the growth via the reaction path in Eq. (1).

The surface chemistry of Al_2O_3 ALD has been studied extensively with FTIR absorption spectroscopy. These measurements confirmed that the surface chemistry was dominated by the $–CH_3$ and –OH groups when employing TMA and H_2O. It is insightful to provide some background information on FTIR spectroscopy before discussing a typical result. To study the surface chemistry of ALD with FTIR absorption spectroscopy, the absorption of infrared radiation by a monolayer of $–CH_3$ or –OH groups needs to be detected. This contribution is small compared to other elements in the optical path absorbing infrared radiation such as the bulk of the substrate on which ALD is performed. To eliminate the contributions by other elements not related to the surface groups and to facilitate the interpretation of the data, it is convenient to work with so called "difference spectra." Such a difference spectrum is calculated from spectra recorded directly before and after a half-cycle. The main difference between the two spectra is the absorption due to the *change* in surface groups; hence, the difference of the two spectra will emphasize these changes. A positive (negative) peak in a difference spectrum indicates the increase (decrease) of the presence a specific surface group. Note that this approach will only reveal species that are *changing*.

Ott *et al.* used this approach to study which surface groups are involved in the growth of Al_2O_3 by ALD.[13] Figure 2 shows the FTIR difference spectra they reported in their work for both the TMA and H_2O half-cycle.[13] For the TMA half-cycle, an increased absorption in the C–H stretch region around 2900 cm^{-1} can be seen. This implies an increase in the number of $–CH_3$ groups on the surface. The negative peak in the O–H stretch region around 3700 cm^{-1} indicates that the number of –OH groups has decreased after TMA exposure. From these observations, it can be inferred that TMA has chemisorbed on the –OH site as described in Eq. (1a).[13,28] For the H_2O half-cycle, the opposite trends are observed involving the same surface groups: After the H_2O exposure, the number of $–CH_3$ groups decreased and the number of –OH groups increased. This indicates that vapor phase H_2O reacted with $–CH_3$ groups, removing the $–CH_3$ groups from the surface and forming –OH groups.[13,28] This observation is in line with Eq. (1b).

Evidence for the gas phase reaction products can also be obtained with FTIR using an alternative measurement

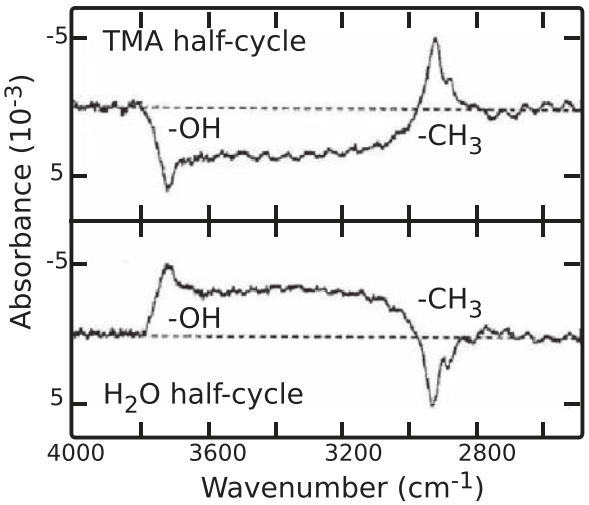

FIG. 2. FTIR absorption spectra showing the change in absorption (i.e., a difference spectrum) related to the change in surface species caused by TMA and H_2O exposure. During the TMA half-cycle, TMA chemisorbs on the –OH groups leading to a decrease in the number of –OH groups (negative peak with respect to the baseline) and an increase in the number of $–CH_3$ groups (positive peak with respect to the baseline) on the surface. During the H_2O half-cycle, vapor phase H_2O reacts with the $–CH_3$ groups which are removed forming new –OH groups. Reproduced with permission from Ott *et al.*, Thin Solid Films **292**, 135 (1997) (Ref. 13).Copyright 1997 Elsevier Science S.A.

scheme. In this scheme, the gas phase reaction products need to be present during the acquisition of one FTIR spectrum and absent during another acquisition. The difference spectrum now contains information about the gas phase species which were present. It is possible to follow the progress of the reactions during a half-cycle, by exposing the surface to multiple consecutive short exposures instead of a single long exposure. Figure 3 shows a set of FTIR spectra identifying the gas phase species formed during ALD. For the TMA half-cycle shown in Fig. 3(a), the first TMA exposure produces mainly CH_4 identified by its unique IR fingerprint.[24] A trace of unreacted TMA can also be seen in the figure.[24,27] Both the second and the third TMA exposure show less CH_4 production and the signature of (unreacted) TMA becomes more evident. During the H_2O half-cycle shown in Fig. 3(b), both gas phase CH_4 and vapor phase H_2O were seen after the first H_2O exposure. Again less CH_4 was produced in the subsequent exposures. These results show that the observed gas phase reaction products are in line with Eq. (1). Moreover, the trends in the amount of gas phase reaction products and the consumption of the precursor and coreactant are in agreement with the self-limiting nature of the ALD reactions.

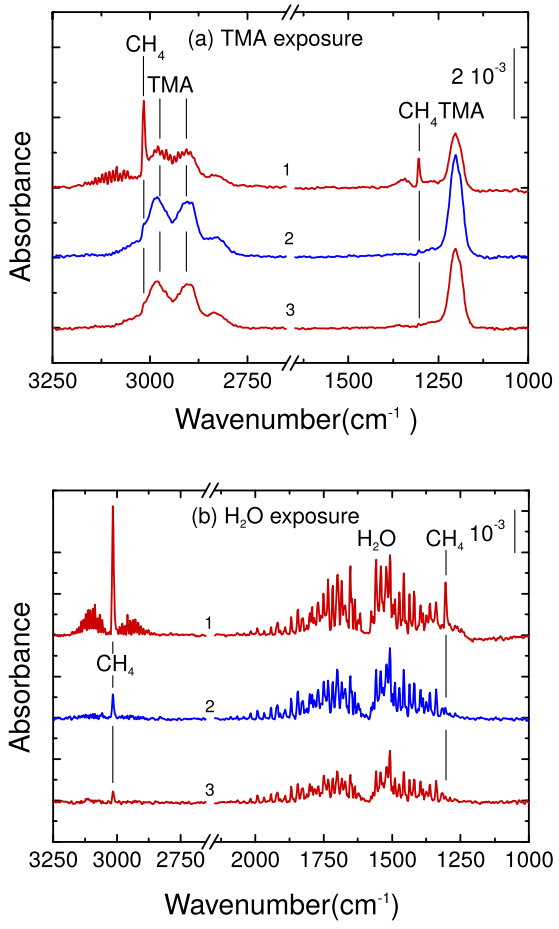

FIG. 3. (Color online) Gas-phase reaction products during ALD of Al_2O_3 measured with infrared absorption spectroscopy for three consecutive precursor and coreactant exposures labeled chronologically in (a) a TMA half-cycle and (b) a H_2O half-cycle. The peak assignments are given in the figure. For both half-cycles, the produced amount of CH_4 decreased with each exposure as a result of the self-limiting nature of the reactions. These experiments were carried out in the home-built reactor ALD-I at 145 °C (Ref. 27).

Complementary to FTIR spectroscopy, QMS is often used to identify and monitor the gas phase reaction products. In QMS, gas phase species are first ionized and subsequently filtered on the basis of their mass-to-charge ratio (m/z). Figure 4 shows the QMS signals recorded during ALD of m/z ratios of 15, 18, and 57 corresponding predominantly to CH_3^+, H_2O^+, and $Al(CH_3)_2^+$, respectively. In this case, the QMS signal strength scales with the partial pressure of the specific gas phase molecule. In the precursor half-cycle, TMA was dosed in five consecutive exposures of 40 ms each. The top panel in Fig. 4 shows the $m/z = 57$ signal corresponding to $Al(CH_3)_2^+$, which is indicative of TMA. The first two exposures of TMA do not give rise to a peak in the $m/z = 57$ signal, indicating that all the TMA is consumed before it can reach the mass spectrometer. This is similar to the result in Fig. 3 where the majority of the TMA was also consumed in the first exposure. Each time the sample was exposed to TMA, an increase in the $m/z = 15$ signal was observed corresponding to CH_3^+. This ion can be produced by ionization of either gas phase CH_4 or gas phase TMA depending on their ionization cross section. For each TMA half-cycle, five consecutive TMA exposures were performed. Assuming that no TMA was consumed in the last exposure and thereby ascribing the entire signal to TMA yields an upper limit for the contribution of TMA to the CH_3^+ signal. From Fig. 4, it can be seen that the TMA contribution to the CH_3^+ signal is indeed small. In the coreactant half-cycle, H_2O was dosed in five consecutive exposures of 100 ms each. The lower panel of Fig. 4 shows the $m/z = 18$ signal indicative of H_2O. Again, gas phase CH_4 was observed as a reaction product. In this half-cycle, there is no

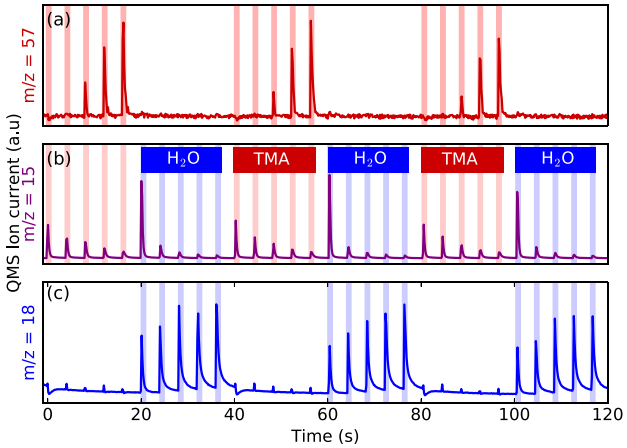

FIG. 4. (Color online) Gas phase species measured with QMS as a function of time for ALD using consecutive exposures of TMA and H_2O. (a) For the TMA half-cycle, the first two TMA exposures (out of five) was fully consumed by the reaction with surface groups, as can be seen from the $m/z = 57$ signal due to $Al(CH_3)_2^+$ indicative of TMA. (b) For both the TMA and H_2O exposures, a peak was observed in the $m/z = 15$ signal that is mainly due to CH_3^+ indicative of CH_4 as a gas phase reaction product. (c) For the H_2O half-cycle, all H_2O exposures resulted in a clear peak in the $m/z = 18$ signal that is mainly due to H_2O^+ and indicative of H_2O. These experiments were carried out in an *Oxford Instruments FlexAL* reactor with a sample and wall temperature of 100 °C.

ambiguity in the assignment of the $m/z = 15$ signal as no TMA was present. The $m/z = 18$ signal shows H_2O molecules reaching the QMS apparatus even in the first exposure. This is different from the TMA half-cycle, where no TMA reached the detector in the first two exposures. This difference is caused in part by the lower reactivity of H_2O toward $–CH_3$ groups than TMA to –OH groups. To recapitulate, the gas phase reaction products measured with both FTIR and QMS are in line with the reactions given in Eq. (1).

A key step in the characterization of an ALD process is to verify that the surface chemistry is indeed self-limiting. This is often done by measuring the influence of the precursor and coreactant exposure on the GPC. If the ALD process is well behaved, the GPC approaches a horizontal asymptotic value for sufficiently long exposures and purge steps, i.e., the GPC shows saturation. Figure 5 shows the variation in the GPC as a function of precursor exposure, coreactant exposure, and purge time measured with spectroscopic ellipsometry (SE).[29] To study the influence of a single parameter in these experiments, all other steps were made sufficiently long to ensure their saturation. The GPC showed saturation for a precursor exposure of ≳20 ms and a coreactant exposure of ≳10 ms. For the purge steps, saturation was observed for purges of ≳1 s. The GPC for the optimized ALD cycle was ∼1.0 Å, a typical value for Al_2O_3 ALD at a deposition temperature of 250 °C.

The deposition temperature has a significant influence on the ALD process.[6,13,30–32] The lowest practical temperature for thermal Al_2O_3 ALD is ∼150 °C. At lower temperatures, the ALD cycle becomes quite long because H_2O is difficult to remove at low temperatures resulting in extremely long purge steps. Also the mass density of the deposited Al_2O_3 decreases significantly for deposition temperatures below 150 °C.[6] For example, Groner *et al*. showed that a deposition at 33 °C requires a cycle time of ∼200 s (compared to, e.g., 4 s) and the mass density of the film is ∼20% less than for films grown at high temperatures.[6] Temperature also has an impact on the GPC of the Al_2O_3 ALD process. The GPC in Fig. 5 was expressed in thickness, labeled here as GPC(nm), which is a suitable parameter if, e.g., a certain thickness is required for an application. Moreover, it can be measured by, e.g. *in situ* SE. Alternatively, the GPC can be expressed as the number of atoms deposited per surface area, labeled as GPC(at). This quantity is more closely related to, e.g., the number of precursor molecules chemisorbing on the surface per cycle. For mechanistic studies, the GPC(at) is therefore more suited. Basically, the GPC(at) can be calculated from the GPC(nm) if the atomic density (atoms/m^3) and the stoichiometry of the film are known. A direct method of determining the GPC(at) is Rutherford backscattering spectrometry (RBS).[7] In RBS, the areal density of a specific atom is measured. Dividing the areal density by the number of ALD cycles used to prepare the film results in the GPC(at). On the other hand, as stated before, the GPC(at) is given by the atomic density multiplied by the GPC(nm). Both the atomic density and the GPC(nm) can be measured with x-ray reflectivity (XRR),[6] or more indirectly with SE using the Lorentz–Lorenz relation.[13,21,30,33] Figure 6 shows the GPC(at) based on the values reported in the literature for both thermal Al_2O_3 ALD and the related plasma-enhanced ALD (PE-ALD) process of Al_2O_3 using the same precursor with a minor correction applied to the Groner *et al*. dataset, see also supplementary material.[34] The temperature trend in the GPC(at) for the thermal process shows an increase with temperature up to ∼200 °C. For temperatures above ∼250 °C, the GPC(at) decreases steadily with temperature. For the PE-ALD process, the GPC(at) decreases monotonically with temperature. The cause of these trends will be discussed later. General consensus is lacking on the exact upper temperature limit at which it is no longer possible to achieve self-limiting growth and hence ALD. However, it has been reported that the precursor starts to decompose above ∼450 °C.[12,35]

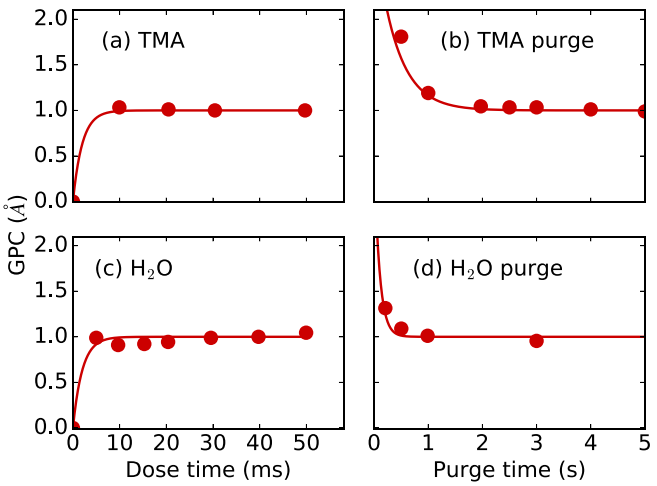

FIG. 5. (Color online) So-called saturation curves for thermal ALD of Al_2O_3 at 250 °C. The growth-per-cycle [GPC(nm)] as a function of (a) the TMA and (c) the H_2O dose and [(b) and (d)] their corresponding purge steps. The lines serve as a guide to the eye. The experiments were carried out in an *Oxford Instruments OpAL* reactor, and the data were taken from Dingemans and Kessels (Ref. 29).

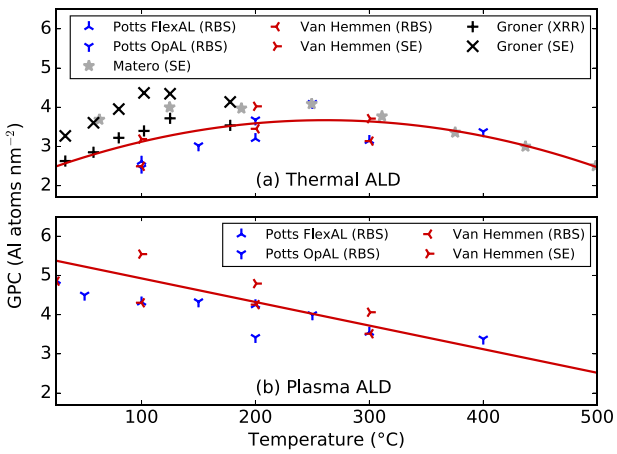

FIG. 6. (Color online) Growth per cycle in terms of Al atoms per surface area [GPC(at)] for (a) thermal and (b) PE-ALD as reported in the literature. For the data obtained with RBS and XRR, the data was used as reported. For works reporting the GPC determined with SE, the GPC(at) was calculated from the reported refractive index and the GPC(nm). The data were taken from Matero *et al*., van Hemmen *et al*., Groner *et al*., and Potts *et al*. (Refs. 6, 7, 21, and 30). The solid line serves as a guide to the eye.

The deposition temperature also influences the density and stoichiometry of the ALD Al_2O_3 films to a certain extent. The Al_2O_3 films deposited by ALD, i.e., typically below 450 °C, are all amorphous. The structure of this amorphous material changes with temperature, going from a local structure similar to that of α-Al_2O_3 at high temperatures to a structure closer to amorphous aluminum oxide hydroxide [AlO(OH)] for deposition at low temperatures.[36] This trend is also reflected in the stoichiometry of the films which are slightly O rich at high temperatures.[6,7,21,32,37] At lower temperatures, the films become even more O rich,[6,7,21,32,36,37] in line with the AlO(OH) structure. The films prepared with thermal ALD are generally carbon free, even when deposited at low temperatures.[21] Furthermore, an increasing amount of H and –OH in the bulk of the films is reported with decreasing temperature.[6,21] The mass density of the Al_2O_3 prepared with ALD is reported to decrease from 3.0 g/cm^3 at 300 °C to approximately 2.8 g/cm^3 at 100 °C.[6,7,21] For comparison, the density of (crystalline) α-Al_2O_3 and γ-Al_2O_3 are 3.99 and 3.97 g/cm^3, respectively.[38]

III. EXPERIMENTAL DETAILS

A. ALD setup and sample preparation

The growth mechanism of ALD was studied using BB-SFG spectroscopy in a purpose-built ALD reactor (see also Fig. 7). The reactor chamber consisted of two parts; both were equipped with a turbomolecular pump (*Pfeiffer TMU 261P*) with an individual backing pump. Both parts reached a base pressure of $<1 \times 10^{-6}$ mbar. The backing pumps were also used as roughing pumps. The ALD precursors [$Al(CH_3)_3$ and $Al(CD_3)_3$] and coreactants (H_2O and D_2O) were dosed into the front part of the reactor with fast ALD valves (*Swagelok 34C-A-GDFG-1KT*) each attached to the reactor with an individual line. The sample was situated at the interface between the two reactor parts and it was heated radiatively from the backside with a Boralectric heating element (*GE Advanced Ceramics ACSF0073 HTR1002*). Sample temperature was computer controlled using a temperature readout from a thermocouple (*Thermocoax 2ABAc05/1m/TI/FIM.K*) glued with thermal paste (*RS 186–3600*) to the back side of the sample as input.

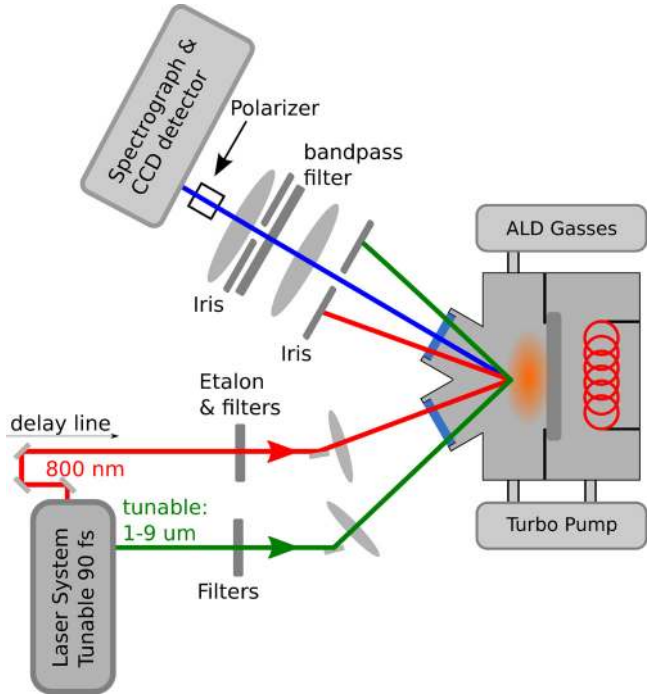

FIG. 7. (Color online) Schematic of the experimental setup consisting of the ALD reactor, the laser system, and the key optical components used for BB-SFG spectroscopy.

The sample used in the BB-SFG experiments consisted of a Si(100) wafer on which a 90 nm thick SiO_2 film was deposited with plasma-enhanced chemical vapor deposition (PE-CVD) for optical enhancement of the BB-SFG signal.

B. BB-SFG spectroscopy and quantification

In BB-SFG spectroscopy, the surface groups are simultaneously irradiated with a spectrally narrow visible pulse and a broadband mid-IR pulse. The visible laser pulses were generated using a regenerative amplifier (*Spectra-Physics Spitfire*) producing pulses with a duration of ~90 fs at a repetition rate of 1 kHz. This amplifier was seeded with a mode-locked oscillator (*Spectra-Physics Tsunami*) and pumped with intracavity doubled, diode-pumped Nd doped yttrium lithium fluoride laser (*Spectra-Physics Evolution 30*). The average output power of *Spitfire* was 1.5 W. From this output beam, 30% of this light was used as the visible pulse in the BB-SFG experiment. To get the desired spectral and temporal shape, the visible light was passed through an etalon (*CVI F1.1–800*). The mid-IR laser pulse was generated from the remaining ~70% of the visible light using an optical parametric amplifier (*Spectra-Physics TOPAS-C*) with an additional difference-frequency mixer. The mid-IR beam and the visible beams were directed toward the ALD reactor, synchronized with a delay line, and focused noncollinearly onto the sample. A separate set of optics was used for each of the two beams. For the mid-IR beam a combination of a positive and a negative CaF_2 lens were used. This combination of lenses improved the numerical aperture and allowed a tighter focus (effective focal length 750 mm). The visible beam, which was much larger in diameter than the mid-IR beam, was focused on the sample with a single lens (focal length 750 mm). A CaF_2 window was used to admit the two pulses into the ALD reactor. After passing through all optical components, the average power was ~5 mW for each of the two laser beams. The two pulses impinged on the sample in a reflection geometry at an angle of incidence ~30° from the surface normal.

The BB-SFG signal exited the reactor through a fused silica window and was filtered spatially (using two irises of ~4 mm) and spectrally (using four *Thorlabs FES0750* filters each with an optical density >5). The *S*-polarized component of the BB-SFG beam was selected with a polarizer and focused on the slit of the spectrometer. The BB-SFG signal was detected with an *Acton Research SP2500* spectrograph and *Princeton Instruments 100B* CCD camera. The polarization combination of the BB-SFG signal recorded in this

work is *Ssp* (*S*-polarized SFG, *s*-polarized visible, and *p*-polarized mid-IR light).

The relative surface coverage ρ of the measured groups was determined from the BB-SFG spectra. The resonant contribution caused by a vibrational mode of a surface group, e.g., the C-H stretch mode of a $-CH_3$ group, was modeled using a Lorentzian line shape. Furthermore, a small nonresonant contribution χ_{NR} had to be included. The spectral shape of the BB-SFG signal $I(\omega)$ for a single resonance was described by

$$I(\omega) \propto \left| \chi_{NR} + \rho \frac{A e^{-i\phi}}{\omega - \omega_{res} \pm \Gamma} \right|^2 I_{vis} I_{ir}, \quad (2)$$

with I_{vis} and I_{ir} the intensity of the visible and mid-IR beams exciting the surface groups. The resonant contribution was described by: A the cross section of the SFG process for the specific resonance, ϕ the phase of the resonance, ω_{res} the resonance frequency, and Γ the broadening of the resonance. The spectra were modeled by fitting this equation to the data using a least-squares algorithm.

IV. RESULTS AND DISCUSSION

A. Basic surface chemistry

The C-H stretch region of the BB-SFG response was probed after the TMA and H_2O half-cycle during steady-state ALD growth of Al_2O_3 at 250 °C. To ensure steady-state growth, five ALD cycles were performed before recording a BB-SFG spectrum. After this preparation, an ALD cycle was performed and a BB-SFG spectrum was recorded after each half-cycle with the mid-IR laser tuned to 2850 cm^{-1} (see Fig. 8). After the TMA half-cycle, the C-H stretch mode of the $-CH_3$ surface groups was indeed observed at 2890 cm^{-1}. After the H_2O cycle, a flat spectral response was recorded in this region, indicating that all the $-CH_3$ groups were removed by the H_2O exposure. The O-H stretch mode of the –OH surface groups (3690 cm^{-1}) falls outside of the spectral region probed with the mid-IR laser tuned to 2850 cm^{-1}. In principle it was possible to tune the laser to a different wavelength and probe the O-H stretch region. However, for such a measurement, the beam path (~10 m) would need to be purged with, e.g., dry nitrogen to remove ambient H_2O. More importantly, it is preferable to probe both $-CH_3$ and –OH groups with the same laser pulses without tuning the laser system, allowing a comparison of the relative $-CH_3$ and –OH peak height eliminating a laborious and error prone calibration procedure. Replacing H_2O with D_2O conveniently shifts the vibrational frequency of the O–H stretch mode into the spectral range probed with the laser tuned to 2850 cm^{-1}. This shift is related to the heavier mass of D compared to H which should shift the stretch mode toward lower wavenumbers by a factor of $\sim\sqrt{M_D/M_H} = \sim \sqrt{2}$.[39] Figure 8 shows the BB-SFG spectra recorded for ALD with either H_2O or D_2O, with all other factors being unchanged. The BB-SFG spectrum for the TMA half-cycle for the TMA/H_2O process was identical to that of the TMA/D_2O process. This demonstrates that the surface chemistry was not affected when H_2O was replaced with D_2O. The –OD groups were successfully detected after the D_2O half-cycle at 2725 cm^{-1}. Note that the spectral position and shape of the resonance indicate that the –OD groups on a surface have negligible H-bridges. Such bonding would induce a shift and a significant broadening (spanning > 200 cm^{-1}) of the peak otherwise.[40,41] To recapitulate, both the $-CH_3$ and the –OD groups were observed with BB-SFG with a sensitivity better than 10% of a monolayer.

To study the influence of temperature on the surface groups, BB-SFG spectra were also collected for ALD at 150 °C using TMA and D_2O. Comparing the BB-SFG spectra recorded after the TMA half-cycle in Fig. 9 for ALD at 150 and 250 °C reveals a stronger $-CH_3$ signal at 150 °C indicating that more $-CH_3$ groups are present on the surface. This was attributed to thermally induced dehydroxylation which increases with temperature, resulting in a lower -OH coverage at high temperatures and therefore a lower TMA uptake.[12] Furthermore, it is known from our earlier work that for ALD of Al_2O_3 at temperatures below ~200 °C there are *persistent* $-CH_3$ groups remaining on the surface after the H_2O half-cycle.[18] The persistent $-CH_3$ groups were also observed in this experiment for ALD at 150 °C and absent at 250 °C. The spectrum recorded after the D_2O half-cycle for ALD at 150 °C clearly showed both $-CH_3$ and –OD groups. The interpretation of the small differences in shape and area of the –OH signal at 150 and 250 °C is not straightforward and beyond the scope of this work.[42]

Replacing TMA with a fully deuterated molecule [D-TMA, $Al(CD_3)_3$] should lead to a shift of the stretch mode of the $-CH_3$ groups by a factor of $\sim\sqrt{2}$ toward lower wavenumbers. Figure 10 shows the signal of the C–D stretch mode of the $-CD_3$ groups which was detected at 2125 cm^{-1} which is indeed shifted by a factor of $\sim\sqrt{2}$ compared to stretch mode of $-CH_3$ at 2890 cm^{-1}. The signal-to-noise

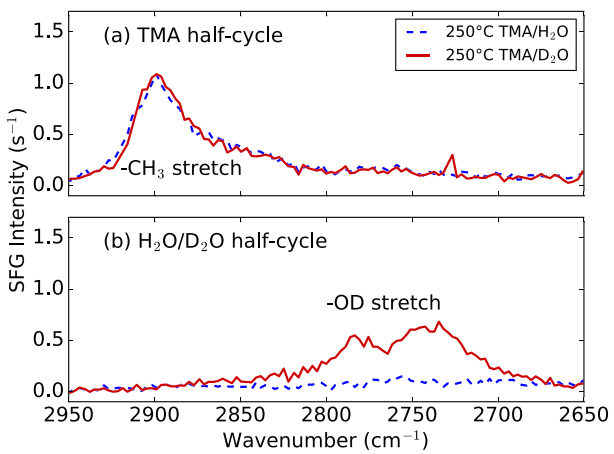

FIG. 8. (Color online) BB-SFG spectra recorded after a TMA and a H_2O or D_2O half-cycle for ALD of Al_2O_3 at 250 °C. (a) The stretch mode of the $-CH_3$ groups was visible after the TMA half-cycle. Replacing H_2O with D_2O shows an identical spectrum for the TMA half-cycle. (b) The stretch mode of the –OH groups after the H_2O half-cycle cannot be observed as it falls outside of the spectral range of the measurement. In the D_2O half-cycle, a broad feature around 2725 cm^{-1} is visible, which is the stretch mode of –OD groups on the surface.

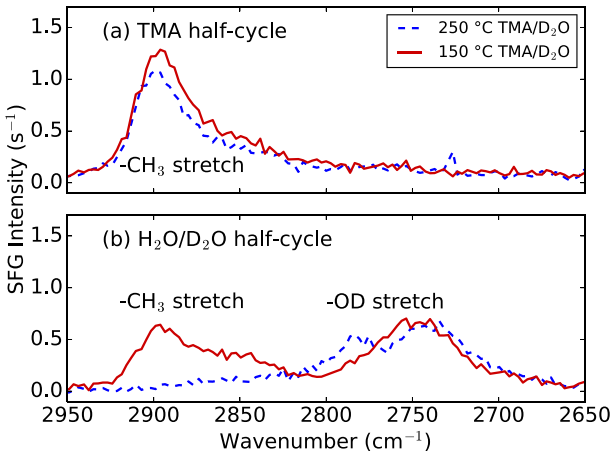

FIG. 9. (Color online) BB-SFG spectra for ALD at 150 and 250 °C using TMA and D_2O. (a) At 250 °C the $–CH_3$ groups appear after TMA exposure and –OD groups appear after D_2O exposure. At 150 °C the ALD process shows a slightly higher $–CH_3$ density after the TMA half-cycle and (b) both –OD and *persistent* $–CH_3$ groups are present on the surface after the D_2O half-cycle.

level is rather poor due to the lower output power of the mid-IR laser at this wavelength used to probe the surface groups. Possibly, the signal-to-noise ratio was reduced even more by a lower SFG cross section due to the deuteration.[39,43] Nevertheless, not only did the $–CD_3$ signal appear at the expected position, it also behaved as described in Eq. (1). The $–CD_3$ signal appeared after the D-TMA half-cycle and disappeared after the D_2O half-cycle. This additional evidence corroborates the assignment of the signal at 2890 cm^{-1} to the C-H stretch mode of $–CH_3$ surface groups.

To summarize, at high temperatures, the chemistry of Al_2O_3 ALD is described accurately by Eq. (1): After the TMA half-cycle, the surface is covered by $–CH_3$ groups. After the H_2O half-cycle, there are only –OH groups on the surface. For ALD at low temperatures, only $–CH_3$ groups were observed after the TMA half-cycle. However, after the H_2O half-cycle, both –OD and *persistent* $–CH_3$ groups were present on the surface.

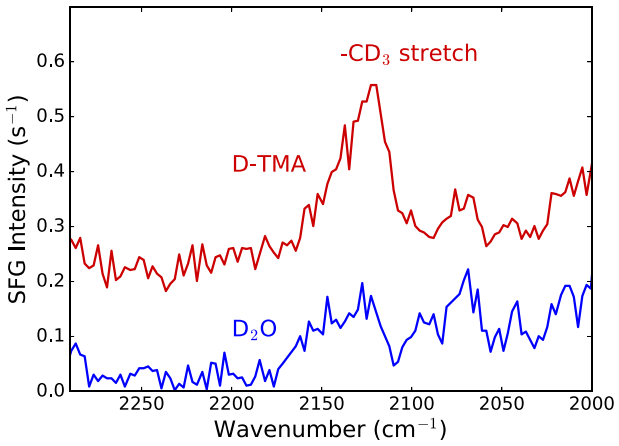

FIG. 10. (Color online) Using D-TMA and D_2O at 200 °C, the stretch mode of the $–CD_3$ groups was detected at 2125 cm^{-1}. The feature appeared after D-TMA exposure and disappeared after D_2O exposure similar to the $–CH_3$ signal observed when using TMA. The signal-to-noise ratio is rather poor due to a relatively low laser intensity at this wavelength.

B. Reaction kinetics

Fundamental insight into the surface reactions ruling ALD can be gained by studying the reaction kinetics and their temperature dependence. By definition, the reaction kinetics describes how the reaction rate depends on the reactant exposure. The reaction kinetics of steady-state ALD were measured for both half-cycles by monitoring the $–CH_3$ signal as a function of precursor and coreactant exposure. Note that for this experiment the central wavelength of the mid-IR laser was re-tuned to obtain the best possible signal-to-noise ratio for the $–CH_3$ signal. Figure 11 shows how the $–CH_3$ signal varied as a function of TMA and H_2O exposure during ALD at 150 °C. For ALD at 150 °C, the surface is covered with both –OH and *persistent* $–CH_3$ groups at the start of the TMA half-cycle. This can be seen in Fig. 11 from the nonzero $–CH_3$ signal at the end of the H_2O half-cycle and at the start of the TMA half-cycle. This surface, terminated with both –OH and $–CH_3$ groups, was exposed to TMA by pulsing the ALD valve for 20 ms. The increase in the intensity of the $–CH_3$ signal in Fig. 11(a) reflected an increase in the amount of $–CH_3$ groups on the surface. This procedure was repeated until the $–CH_3$ signal no longer increased, i.e., saturation was reached. The surface at the end of the TMA half-cycle is the starting surface for the subsequent H_2O half-cycle. A BB-SFG spectrum was recorded at the beginning of the H_2O half-cycle [see also the top spectrum in Fig. 11(b)]. Then, the surface was exposed to vapor phase H_2O by pulsing the ALD valve for 40 ms, resulting in the removal of a part of the $–CH_3$ groups. This procedure was repeated until the $–CH_3$ coverage no longer changed indicating that saturation was reached. The $–CH_3$ groups still present on the surface were no longer reactive toward H_2O, i.e., *persistent* $–CH_3$ groups.

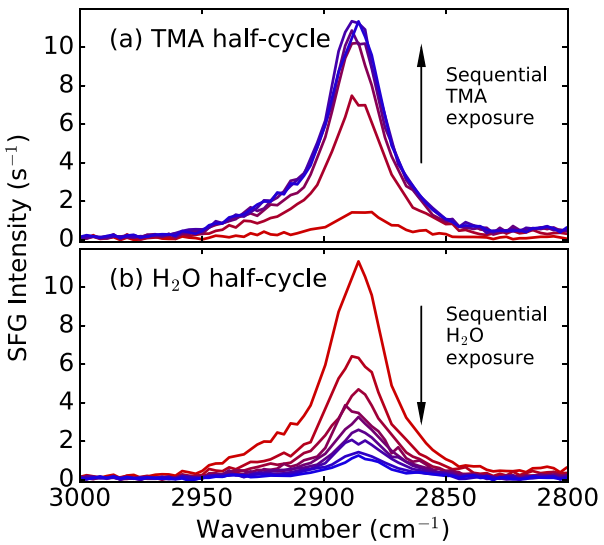

FIG. 11. (Color online) BB-SFG spectra showing the stretch mode of the $–CH_3$ groups on the surface during ALD at 150 °C. The number of $–CH_3$ groups is reflected by the strength of the resonance at 2890 cm^{-1}. (a) During the TMA half-cycle, the number of $–CH_3$ groups increased until saturation was reached. (b) During the H_2O half-cycle, initially the H_2O exposure removed $–CH_3$ from the surface. However, this reaction saturated even though there were $–CH_3$ groups on the surface. These $–CH_3$ groups were no longer reactive with H_2O and were labeled as *persistent* $–CH_3$ groups.

Figure 12 shows the relative –CH_3 density θ_{CH} as a function of the duration of the H_2O exposure. The relative –CH_3 density was determined from the BB-SFG spectra in Fig. 11 by fitting the spectra with the appropriate peak shape.[18,23,44] The experiment was performed at temperatures between 100 and 300 °C to determine how temperature affected the reaction kinetics. For high temperatures, the reaction in the H_2O half-cycle was fast and removed all the –CH_3 groups, whereas for lower temperatures, the reaction slowed down and saturated before all the –CH_3 groups were removed, resulting in the aforementioned *persistent* –CH_3 groups. An additional check with a prolonged H_2O exposure of 400 and 800 ms exposure (not shown) was performed at 150 °C and did not reveal an additional –CH_3 removal.

The reaction kinetics plotted in Fig. 12 describe the relation between the H_2O flux, Γ_{H_2O}, and the change in –CH_3 coverage, $d\theta_{CH}/dt$. The reaction in the H_2O half-cycle, given by Eq. (1b), can be described by the following equation:

$$\frac{d\theta_{CH}}{dt} = -\sigma_{H_2O}\theta_{CH}\Gamma_{H_2O}, \tag{3}$$

in which σ_{H_2O} is the reaction cross section. The reaction cross section (with units cm^2) is closely related to the initial reaction (or sticking) probability $S_0 = \sigma N_{CH}^{full}$, with N_{CH}^{full} the absolute –CH_3 coverage after a saturated TMA step. S_0 represents the probability that a H_2O molecule reacts with a –CH_3 group when it impinges on a fully –CH_3 covered surface. The solution of Eq. (3) is given by an exponential function $[\exp(-\sigma_{H_2O}\Gamma_{H_2O}t)]$ and describes the reaction kinetics at high temperatures. The decay seen at low temperatures (below 200 °C) cannot be described by this exponential function alone. The reaction saturates before all the –CH_3 groups are removed, i.e., the *persistent* –CH_3 groups on the surface. This means that at low temperatures the reaction kinetics cannot be described with a single first-order reaction with a constant cross section.

To explain these reaction kinetics, two models are proposed. Either there are two kinds of –CH_3 groups or the reactivity of the –CH_3 groups is coverage dependent. In the first model, each of the two kinds of –CH_3 groups has its own reaction, and Eq. (1b) consists in fact of two parallel reaction paths. The reaction for the *reactive* type of –CH_3 has a low activation energy and occur at typical ALD temperatures. The reaction for the *persistent* –CH_3 groups has a higher activation energy such that this reaction only occurs at elevated temperatures resulting in *persistent* –CH_3 at low temperatures. In this model, the relative coverage of the *reactive* groups is described by an exponential function of the H_2O exposure (assuming this reaction is a first order reaction). The *persistent* groups are described by a variable at low temperatures and by exponential function at high temperatures. This model was also discussed in our previous work.[18] The underlying microscopic cause for the two types of –CH_3 groups might be due to different reactivity of various surface sites of the –CH_3 groups, analogous to reactions at step edges and terraces on crystalline surfaces. On these ideal surfaces, large differences in reactivity are observed. For example, the reaction rate of H_2 dissociation on a Pt surface depends on the crystal face, e.g., Pt(100) versus Pt(111), and on the step-edge density.[45]

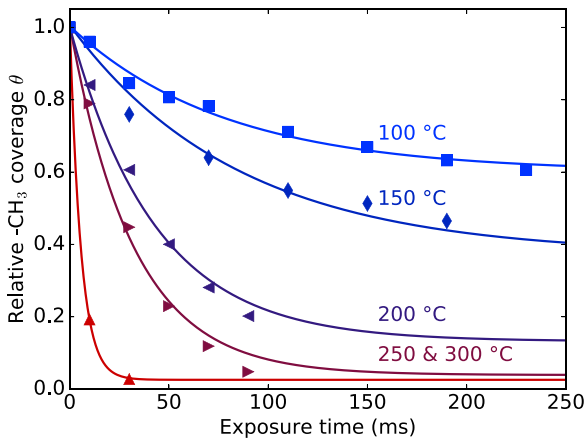

FIG. 12. (Color online) Relative –CH_3 coverage as a function of H_2O exposure for ALD at 100 up to 300 °C obtained from fits to the BB-SFG spectra. At high temperatures, the reaction is fast and removes all –CH_3. At lower temperatures, the reaction slows down and saturates before all –CH_3 is removed leaving *persistent* –CH_3 on the surface.

The second model, a coverage dependent reactivity of the –CH_3 groups, is also known from the field of surface science. This occurs, for example, for the oxidation of CO on a rhodium surface where a strong coverage dependence in the reactivity was found.[46,47] A similar effect was reported for the dimethylamine precursor in CVD, where the adsorption of the precursor showed a coverage dependent reaction cross section.[48] Moreover, the support for the existence of this mechanism in ALD can be found in recent *ab initio* work by Shirazi and Elliott.[20] In their DFT simulations, isolated –CH_3 groups are not reactive toward H_2O (i.e., a high activation energy). On the other hand, clusters of three –CH_3 groups are reactive toward H_2O. If the microscopic reaction cross section depends on number of neighboring –CH_3 groups, it is likely that the macroscopic cross section depends on the surface coverage. This model, assuming a nonconstant reaction cross section $\sigma(\theta)$, leads to an change in Eq. (3) for the H_2O half-cycle, substituting σ_{H_2O} by $\sigma_{H_2O}(\theta_{CH}) = f(\theta_{CH})$. The coverage dependent cross section can be calculated from the data in Fig. 11 by rearranging Eq. (3). Note that the unknowns in the resulting expression for $\sigma_{H_2O}(\theta_{CH})$—namely, Γ, θ_{CH}, and $d\theta_{CH}/dt$—were all measured in the experiment which means that σ can be calculated from this data set. Figure 13 shows the reaction cross section of the H_2O half-cycle as a function of surface coverage calculated from the data in Fig. 12. For ALD at higher temperatures, the cross section is independent of the surface coverage. For lower temperatures, the value of the cross section decreases, and below 200 °C, the cross section shows a coverage dependence. For comparison, the reaction cross section of the TMA half-cycle reported in our previous work was $\sigma = 6.5 \times 10^{-18}$ cm^2. For TMA, the cross section was found to be independent on surface coverage, did not vary with temperature in the investigated range between 100 and 300 °C, and is 2 orders of magnitude larger than that of H_2O.[18]

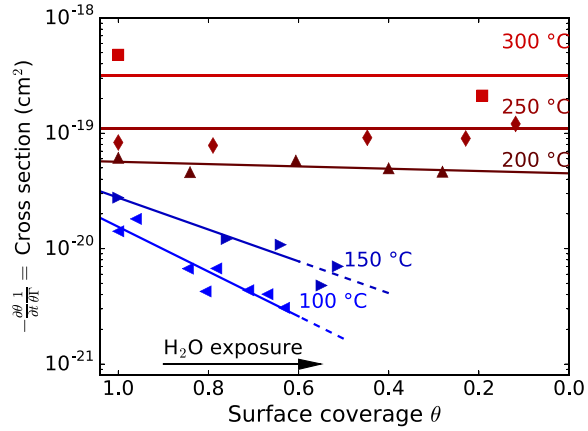

FIG. 13. (Color online) Reaction cross section determined for the H_2O half-cycle as a function of surface coverage for ALD at 100 up to 300 °C. At high temperatures, the cross section is constant resulting in an exponential decrease of $–CH_3$ coverage as function of H_2O dose. Below 200 °C the cross section clearly depends on the surface coverage. Due to the fast reaction at high temperature, only two data points were available at 300 °C. The solid lines are a guide to the eye.

In the context of the coverage dependent reactivity model, the temperature dependence of the reactivity of the $–CH_3$ groups toward H_2O can be described in terms of an activation energy. This temperature dependence, for a reaction dominated by single rate limiting step, is described by the Arrhenius equation. This means that the reaction cross section is proportional to $\exp(-E_a/(k_bT))$ with k_b the Boltzmann constant and E_a the activation energy of the reaction. Figure 14 shows a so-called Arrhenius plot of the reaction cross section (taken from Fig. 13) versus the reciprocal temperature. For $\theta_{CH}=1$, the reaction cross sections do indeed fall on a straight line in the Arrhenius plot yielding an activation energy of $E_a=0.27$ eV. Note that also the sticking probability S is often used in the Arrhenius plot to determine the activation energy. Strictly speaking, the use of σ yields results that are the closest to the microscopic description of the reaction, but the results with S are comparable (varying by ~0.01 eV). The activation energy was also determined for surface coverages $\theta_{CH}<1$ with the same procedure using the reaction cross sections at other coverages taken from Fig. 13. As shown in Fig. 14, an increasing E_a was found with decreasing $–CH_3$ coverage, with, for example, an activation energy of $E_a=0.43$ eV at $\theta_{CH}=0.66$. This increase in E_a for decreasing $–CH_3$ surface coverage underlines the coverage dependent reactivity model.

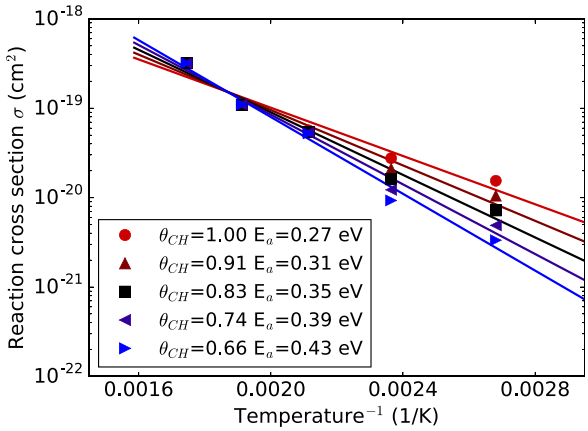

FIG. 14. (Color online) Arrhenius plot of the reaction cross section σ vs reciprocal temperature for various surface coverages.

The activation energy found for $\theta_{CH}=1$ can be directly compared to the predictions made by DFT simulations for the activation energy of clusters of multiple $–CH_3$ groups. Shirazi and Elliott reported an activation energy of 0.25 eV for a cluster of three CH_3 groups undergoing the reaction $3Al-CH_3+H_2O\rightarrow 2Al-CH_3+Al-OH+CH_4$.[20] Similarly, Weckman and Laasonen found an activation energy of 0.44 eV for two CH_3 groups undergoing the reaction $Al-(CH_3)_2+H_2O\rightarrow Al-CH_3OH+CH_4$.[49] The interpretation of the activation energy at coverages $\theta_{CH}<1$ is somewhat less straightforward. For $\theta_{CH}<1$, the density of $–CH_3$ groups varies over the surface with some spots having clusters of several $–CH_3$ groups while others spots have only isolated $–CH_3$ groups. The ratio between the coverage of isolated $–CH_3$ groups to the coverage of clusters of multiple $–CH_3$ groups also varies with the temperature. This means that the experimental activation energy should be viewed as an average activation energy over several types of $–CH_3$ groups which cannot be associated with one specific reaction in the DFT simulations. Nevertheless, the trend in the activation energy can be interpreted. At high surface coverages, virtually no isolated $–CH_3$ groups are present and the activation energy corresponds with the aforementioned activation energy for clusters with multiple $–CH_3$ groups. At lower $–CH_3$ coverages, a higher fraction of isolated $–CH_3$ groups will be present. For isolated $–CH_3$ groups, both Shirazi and Elliott and Weckman and Laasonen report that these are not reactive toward H_2O implying an activation energy >1.47 eV based upon arguments in the former work.[20,49] Therefore, the increase observed in the experimental activation energy with decreasing $–CH_3$ coverage is in line with the expected increase in the fraction of unreactive isolated $–CH_3$ groups.

To summarize, at high temperatures, the reactions in the H_2O half-cycle obey first-order reaction kinetics. Below 200 °C, the reaction kinetics can no longer be described as a first-order reaction and *persistent* $–CH_3$ groups remain on the surface. Two possible models were proposed to account for these observations: (1) There are two types of $–CH_3$ groups each with its own reactivity. (2) The reactivity of the $–CH_3$ groups depends on the surface coverage at low temperatures. Both models are established in the field of surface science, they can equally well describe the data, and both models are not necessarily mutually exclusive. However, we prefer the coverage dependent model because this effect has been observed in the related deposition process of CVD and was it actually predicted for the Al_2O_3 ALD process by *ab initio* DFT simulations.

C. Quantification of the $–CH_3$ density

The relative $–CH_3$ coverage after the TMA and the H_2O half-cycle was measured with BB-SFG spectroscopy for

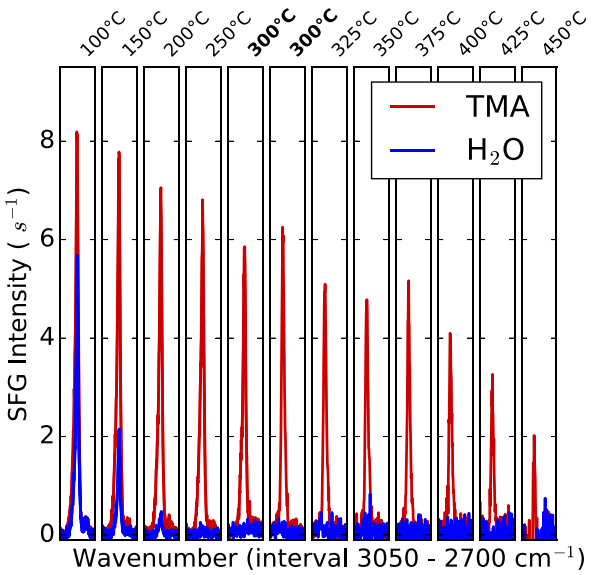

FIG. 15. (Color online) BB-SFG spectra of the $–CH_3$ signal after a saturated TMA and H_2O exposure for ALD between 100 and 450 °C. This data were collected in two separate experimental runs (100–300 and 300–450 °C).

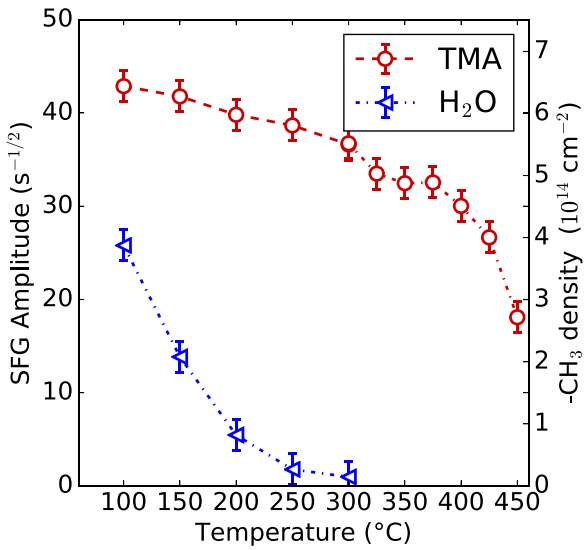

FIG. 16. (Color online) BB-SFG amplitude of the $–CH_3$ signal after the TMA and H_2O half-cycle as a function of substrate temperature obtained from fit of the BB-SFG spectra in Fig. 15. (Right axis) The corresponding absolute $–CH_3$ coverage is also given (see text). At low temperatures, the *persistent* $–CH_3$ groups after the H_2O exposure are visible. The density of *persistent* $–CH_3$ groups was determined from fits to the saturation curves in Fig. 12 for better accuracy. Above 400 °C, effects such as precursor decomposition and precursor desorption might affect the data.

ALD between 100 and 450 °C. At each temperature, five ALD cycles were performed to ensure steady-state growth at that temperature. During the subsequent ALD cycle, BB-SFG spectra were collected after each half-cycle. Then, the temperature was raised by 50 °C, and the measurement procedure repeated after the temperature had settled. It was not practical to simultaneously investigate the reaction kinetics and determine the $–CH_3$ coverage in a single experiment. BB-SFG spectra can only be compared if the optical alignment of the setup remained unaltered. The daily adjustments to the setup limited the number of spectra which could be measured in a single run. To cover a wider temperature range in a single run, spectra were only collected after a saturated half-cycle. With this approach, it was possible to measure the $–CH_3$ coverage from 100 up to 300 °C in one run and from 300 up to 450 °C in a second run. By measuring the $–CH_3$ coverage at 300 °C twice, the influence of possible changes to the optical alignment could be determined. The spectra recorded in this fashion are shown in Fig. 15. For the TMA half-cycle, a gradual decrease of the $–CH_3$ signal with temperature was observed. Comparing the spectra for the TMA half-cycle recorded at 300 °C revealed a small difference in signal strength. For the H_2O half-cycle, *persistent* $–CH_3$ groups were observed at low temperatures.

The relative $–CH_3$ density was determined by fitting the spectra in Fig. 15. Because the two data sets were measured on different days, the two series were joined by scaling the high temperature data such that the extracted $–CH_3$ coverage at 300 °C overlap. The SFG amplitude, which is proportional to the $–CH_3$ density, is plotted on the left axis of Fig. 16. This data were made absolute, i.e., calibrated, by assuming a $–CH_3$ areal density of $5.5 \times 10^{14}\,cm^{-2}$ after the TMA half-cycle for ALD at 300 °C. This assumption is based upon data presented by Rahtu *et al.*, indicating that 1.5 $–CH_3$ groups per Al atom are left after TMA chemisorption at this temperature combined with the GPC(at) of $3.6\,nm^{-2}$.[16] Care was taken to select an appropriate temperature for the calibration procedure as the accuracy of the data is only as good as the calibration. At 300 °C, the calibration data are not affected by low temperature effects such as precursor condensation and persistent surface groups or by high-temperature effects such as precursor decomposition. The right axis of Fig. 16 shows the absolute $–CH_3$ density as a function of temperature for both half-cycles resulting from this procedure. Note that the trend in the relative $–CH_3$ data is independent of the calibration. The $–CH_3$ density after the TMA half-cycle decreases with temperature up to 400 °C, dropping off more rapidly above 400 °C. The trend up to 400 °C can be attributed to temperature induced dehydroxylation leading to a reduction of the density of the –OH groups.[12] The sharp drop can be a combination of decomposition of the chemisorbed TMA, e.g., demethylation, and precursor desorption.[12,35] For the H_2O half-cycle, the persistent $–CH_3$ groups are observed at low temperatures and absent above ~200 °C.

The temperature trend in the $–CH_3$ coverage yields insight into the mechanism causing the self-limiting nature of the TMA half-cycle. For Al_2O_3 ALD, two key mechanisms have been proposed: (1) Steric hindrance. (2) Depletion of "reactive sites."[14] There are proponents for both mechanisms. For example, Puurunen attributed the self-limiting nature of the surface reactions in the TMA half-cycle to steric hindrance.[14] On the other hand, Shirazi and Elliott concluded from their DFT simulations that for the TMA half-cycle the depletion of undercoordinated oxygen sites is the cause of saturation.[20] Both the trend in the $–CH_3$ coverage with temperature and the absolute values of the coverage point toward the depletion of reactive sites. The absolute $–CH_3$ densities reached after the TMA half-cycle,

$\leq 6\,nm^{-2}$ as shown in Fig. 16, are not high enough for steric hindrance. For example, on Si(111) densities as high as eight $–CH_3$ groups per nm^2 have been observed.[50,51] A stronger argument, not depending on the difficult to measure absolute densities, can be found in the temperature trend of the $–CH_3$ density in Fig. 16. For small and immobile surface groups such as the $–CH_3$ groups, the surface area that these groups occupy is temperature independent.[14] This implies that if steric hindrance is the limiting factor, the same $–CH_3$ coverage should be observed at all temperatures. If, for the sake of argument, it is assumed that steric hindrance is the limiting factor at 100 °C and it follows that at higher temperatures a different mechanism must be responsible for the self-limiting behavior. Apart from steric hindrance, the self-limiting nature of the TMA half-cycle can be caused by depletion of reactive sites. This can be subdivided into two categories: (1) Depletion of protons/H-atoms. (2) Depletion of under-coordinated O atoms. The first factor, depletion of protons, can be ruled out from the fact that these Al_2O_3 films are known to contain a significant amount of hydrogen, partly in the form of –OH in the bulk of the film.[21,52,53] This leaves the depletion of under-coordinated O sites as the likely reason for the self-limiting nature of the TMA half-cycle which is in agreement with mechanism proposed by Shirazi and Elliott.[20]

Another topic that can be addressed with this data is the chemisorption of TMA on the -OH groups. TMA can chemisorb on a –OH covered surface in several configurations: TMA can chemisorb monofunctionally, i.e., react with a single -OH groups leaving two $–CH_3$ groups attached to the Al atom. Alternatively, TMA can chemisorb bifunctional, i.e., react with two -OH groups leaving a single $–CH_3$ group attached to the Al atom. It is not likely that TMA reacts with three -OH groups upon chemisorption.[20,49] The number of remaining $–CH_3$ groups per Al after chemisorption was calculated from the change in $–CH_3$ groups $\Delta\theta_{CH}$ during the TMA half-cycle divided by the number of Al atoms deposited per surface area. The GPC(at) data were not available for the temperature range used in this work from a single source, and therefore, the data was taken from Groner *et al.* and Matero *et al.* using the XRR and SE data, respectively.[10,30] The $\Delta\theta_{CH}$ was calculated from the data in Fig. 16. For the thermal ALD process at low temperature, $\Delta\theta_{CH}$ equals the coverage reached after TMA minus the *persistent* $–CH_3$ coverage. At higher temperatures, no *persistent* $–CH_3$ are present, and $\Delta\theta_{CH}$ is equal to the coverage reached in the TMA half-cycle. Figure 17 shows the $\Delta\theta_{CH}$ to Al ratio for the Al_2O_3 ALD process. At low temperatures, TMA chemisorbs bifunctionally, i.e., with one $–CH_3$ group remaining after chemisorption. The number of $–CH_3$ groups remaining after TMA chemisorption gradually increases toward 1.5 for higher temperatures. The related process of PE-ALD of Al_2O_3 can be treated in a similar fashion. For the PE-ALD process, it is expected that even at low temperatures the plasma is reactive enough to completely remove all the $–CH_3$ groups. This was demonstrated in our previous work, where the GPC(at) of the PE-ALD process could be predicted accurately from the $–CH_3$ coverage with this

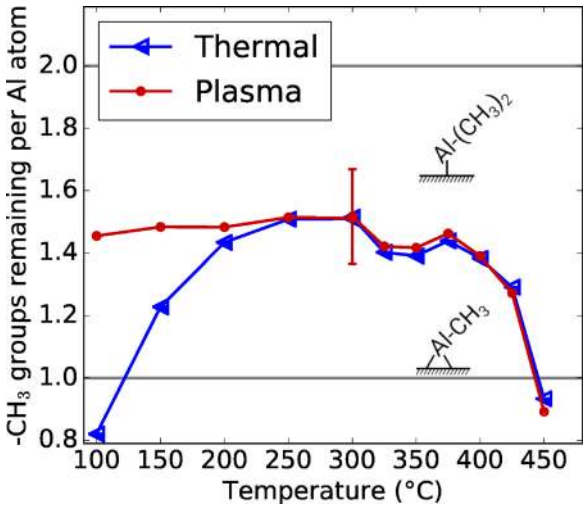

FIG. 17. (Color online) Number of remaining $–CH_3$ groups attached to Al after TMA chemisorption, calculated by dividing the $–CH_3$ coverage (Fig. 16) by the number of Al atoms deposited per cycle (Fig. 6). The thermal process shows a trend toward bifunctional adsorption when going to low temperatures, i.e., the Al atom is twofold coordinated to O and has a single $–CH_3$ group. The related PE-ALD process with O_2 plasma shows a constant number of remaining $–CH_3$ groups after chemisorption as a function of temperature. Above 400 °C, thermal decomposition and desorption of TMA might influence the result for both thermal and plasma ALD.

assumption.[18] Figure 17 also shows the $–CH_3$ to Al ratio for PE-ALD of Al_2O_3. For the PE-ALD process, 1.5 $–CH_3$ groups remain attached to the Al atom after chemisorption. The number of $–CH_3$ groups remaining on the surface after the chemisorption of TMA is independent of temperature up to 400 °C for PE-ALD. Above this temperature, precursor decomposition and desorption might affect the data.

The trend observed for thermal ALD could be explained by a cooperative effect in TMA chemisorption proposed by Shirazi and Elliott.[20] Their DFT results show that when a single TMA molecule chemisorbs on a fully –OH covered surface, it is likely to adsorb monofunctionally. On the other hand, if there is already TMA chemisorbed on the surface, new TMA can adsorb bifunctionally. A similar mechanism could be responsible for the transition from monofunctional to bifunctional chemisorption seen for the thermal ALD process at lower temperatures. At low temperatures, the presence of persistent $–CH_3$ ensures that TMA can chemisorb bifunctionally. At higher temperatures the surface starts out –OH covered and no $–CH_3$ groups are present. Therefore, TMA chemisorbs monofunctionally initially. The chance of bifunctional chemisorption increases with TMA uptake because the already chemisorbed TMA allows new TMA to chemisorb bifunctionally. The average of the monofunctional and bifunctional adsorption could result in the average of 1.5 $–CH_3$ groups per Al atom as observed at high temperatures.

To summarize, from the quantification of the $–CH_3$ coverage, it was possible to deduce that the self-limiting nature of the TMA half-cycle is caused by depletion of under-coordinated O sites. Moreover, for thermal ALD at low temperatures, it was shown that TMA retains one of its $–CH_3$ ligands after chemisorption. This increases to 1.5 $–CH_3$ ligands at higher temperatures.

D. Carbon incorporation

The Al_2O_3 films have been reported to be carbon-free even when deposited at low temperatures.[6,7,21,32] This suggests that the *persistent* $–CH_3$ groups are not incorporated into the film. Therefore, a dedicated experiment was designed to test the hypothesis that $–CH_3$ groups are not incorporated into the film. This was done by intentionally leaving $–CH_3$ groups on the surface by not saturating the H_2O half-cycle for ALD. Two samples were prepared by performing 300 cycles of ALD of Al_2O_3 at a deposition temperature of 200 °C. The first sample, labeled "saturated," consisted of a Si(100) substrate on which an Al_2O_3 film was deposited using the normal process parameters with each process step in saturation. The preparation of the second sample differed only in the duration of the H_2O exposure. The H_2O exposure was chosen to be roughly half of the exposure needed for saturation. This sample was labeled "unsaturated." The film thickness and optical properties of the Al_2O_3 films after deposition were determined with SE and are listed in Table I. The Al_2O_3 film thickness of the unsaturated sample is roughly 60% of the Al_2O_3 thickness found for the saturated sample. For both samples, a similar refractive index was found for the Al_2O_3 film, which is an indication of a similar atomic density. This shows that indeed the H_2O exposure was not saturated for the unsaturated sample but that nevertheless high quality Al_2O_3 was grown in both cases.

The elemental composition of both the samples was analyzed by XPS. The Al2p, C1s, and O1s contribution were measured, and the atomic O to Al ratio and the C content of the material were calculated from the area of the peaks using the appropriate sensitivity factors. A depth profile was made by stepwise sputtering the Al_2O_3 film with Ar ions, measuring an XPS spectra after each sputter step. The [O] to [Al] atomic ratio and the atomic C percentage are shown in Fig. 18 as a function of etch time. At the surface (before the first etch step), adventitious carbon was observed, which is not related to the ALD process. From the first etch step on, the carbon signal for both samples was below the detection limit of the setup which is ~1%. The Al_2O_3 layer was stoichiometric throughout the film with an O to Al ratio of 3:2, in agreement with what is reported for Al_2O_3 ALD at this temperature.[6,21]

For comparison, the expected C content of the unsaturated sample was calculated assuming the worst-case scenario, i.e., full incorporation of unreacted $–CH_3$ groups. Judging from the 40% reduction of the GPC(nm), roughly 40% of $–CH_3$ groups were left on the surface after the H_2O half-cycle during ALD on the unsaturated sample. For each Al atom which is deposited, ~1.5 $–CH_3$ groups will be on the surface after TMA chemisorption. For the unsaturated sample, this means that 0.6 $–CH_3$ groups per Al atom will be left on the surface after the unsaturated H_2O exposure. If all of these C atoms would be incorporated, the stoichiometry of the film would be significantly affected. The composition would be: 32 at. % Al, 19 at. % C, and 48 at. % O. The carbon content was evidently much lower for the unsaturated sample. Moreover, there were no significant differences between the saturated and unsaturated samples with respect to film composition. In short, from this experiment, it can be concluded that $–CH_3$ groups remaining on the surface after the H_2O exposure have a relatively low probability to be incorporated into the film. Most likely, the unreacted $–CH_3$ groups have a chance to react in subsequent coreactant half-cycles. This is of interest for, e.g., industrial applications where ALD is occasionally operated with reduced (subsaturation) precursor and coreactant exposures to optimize the efficiency of precursor usage and the throughput of the ALD system.[36] This approach might affect uniformity and conformality, but it does not necessarily lead to carbon incorporation.

One of the reasons for the absence of carbon incorporation might be related to the specific chemistry of this ALD process. Two plausible mechanism of carbon incorporation for processes such as thermal ALD of Al_2O_3 are (1) incorporation of unreacted precursor ligands and (2) incorporation of carbon containing reaction intermediates formed from the precursor ligands in the coreactant half-cycle. The first cause was ruled out by the aforementioned XPS experiment that showed negligible incorporation of surface $–CH_3$ groups in the film. The second cause is not expected to occur in

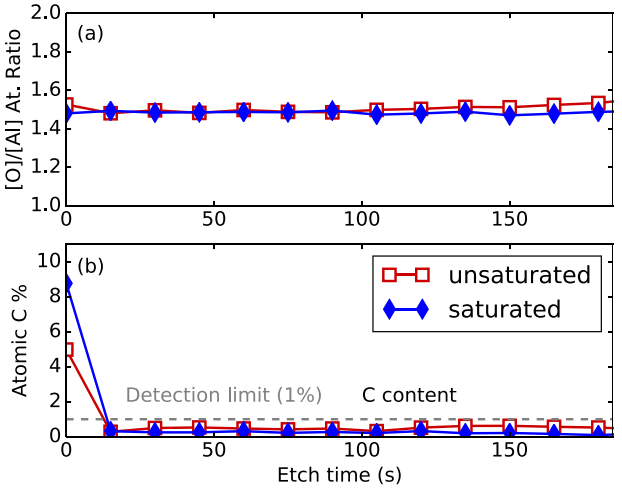

FIG. 18. (Color online) XPS depth profile of two samples with an ALD Al_2O_3 film on Si(100) prepared at 200 °C. The sample labeled saturated was prepared using an ALD recipe where both half-cycles were fully saturated. The sample labeled unsaturated was prepared with the same recipe with a shortened H_2O exposure which resulted in ~60% of the normal GPC. (a) Both films were stoichiometric throughout. (b) In both cases, the carbon content was below the XPS detection limit. The carbon seen at t = 0 is adventitious carbon unrelated to the ALD process. The samples were prepared in an *Oxford Instruments FlexAL* and examined with a *Thermo Scientific K-Alpha* XPS.

TABLE I. Film thickness, refractive index, and GPC determined with spectroscopic ellipsometry for two samples deposited by 300 cycles of ALD. The sample labeled saturated was prepared using an optimized ALD process, while the sample labeled unsaturated was prepared with the same process with a smaller H_2O dose such that the H_2O dose was insufficient to reach saturation.

Sample	Thickness (nm)	GPC (Å)	n 589 nm
Saturated	30.0	1.00	1.67
Unsaturated	16.5	0.55	1.67

thermal ALD of Al_2O_3 because there are no stable carbon containing reaction intermediates expected or known for the reaction in the H_2O half-cycle described by Eq. (1b). The impact of the presence of a carbon containing reaction intermediates is best illustrated by the related PE-ALD process of Al_2O_3 using TMA and an O_2 plasma as the coreactant. For this ALD process, it has been shown that stable carbon containing reaction intermediates exist in the form of a carbonate.[24,25] These carbonates are quickly formed at the beginning of the O_2 plasma half-cycle and gradually combusted by a prolonged O_2 plasma exposure.[24,25] For Al_2O_3 films prepared using an O_2 plasma duration just sufficient for GPC(nm) saturation, a significant amount of C incorporation is reported.[53,54] On the other hand, virtually C free films are deposited with a similar GPC(nm) for the same process using a prolonged O_2 plasma exposure.[53,54] This trend clearly points toward the carbonates as the main source of the carbon incorporated into the Al_2O_3 film grown by PE-ALD. The carbon incorporation during PE-ALD is probably exacerbated by TMA readily chemisorbing on the carbonates.[24,25] To conclude, this example highlights the impact that stable carbon containing reaction intermediates can have on carbon incorporation by comparing the related PE-ALD and thermal ALD processes for Al_2O_3.

V. CONCLUSION

The growth mechanism of the prototypical ALD process of Al_2O_3 was studied with BB-SFG spectroscopy. Several dedicated experiments were performed to elucidate several key aspects of the ALD process: the reaction kinetics, the origin of the self-limiting nature of the surface reactions, the number of -OH groups consumed by the chemisorption of TMA, and the apparent paradox between *persistent* $–CH_3$ groups at low temperatures and negligible carbon incorporation into the Al_2O_3 films.

The overall surface chemistry was monitored for ALD using either TMA or $Al(CD_3)_3$ (D-TMA) as precursor and H_2O or D_2O as coreactant. Comparing BB-SFG spectra of the C-H stretch region using TMA and H_2O versus TMA and D_2O at 250 °C demonstrated that at this temperature the ALD process showed virtually ideal behavior: TMA chemisorbs on the –OH sites and H_2O is reactive enough to remove all $–CH_3$ groups. At 150 °C, TMA did chemisorb on the –OH groups. However, H_2O was not reactive enough at this temperature to remove all $–CH_3$ groups. Both –OD groups and *persistent* $–CH_3$ groups were present on the surface after the D_2O half-cycle. Replacing TMA with D-TMA showed the typical isotope shift in the C-H/C-D stretch mode of the $–CH_3$ groups. These experiments established that both the $–CH_3$ and the –OD groups could be monitored with submonolayer sensitivity with BB-SFG spectroscopy.

The reaction kinetics of the growth mechanism was investigated with BB-SFG spectroscopy by monitoring the $–CH_3$ coverage during the H_2O half-cycle. At high temperatures, the reaction during the H_2O half-cycle was fast, removed all $–CH_3$ groups, and obeyed first-order reaction kinetics. At lower temperatures, the reaction slowed down and *persistent* $–CH_3$ groups remained on the surface. The initial sticking probability and the reaction cross section were quantified. An initial sticking probability $S_0 = 1 \times 10^{-4}$ (cross section $\sigma = 1 \times 10^{-18}$ cm^2) was found for the reactions in the H_2O half-cycle at 300 °C. This decreased rapidly with temperature, with an initial sticking probability of $S_0 = 1 \times 10^{-6}$ (cross section $\sigma = 1 \times 10^{-20}$ cm^2) at 100 °C. For comparison, the initial sticking probability and reaction cross section in the TMA half-cycle reported in our previous work was $S_0 = 2 \times 10^{-3}$ and $\sigma = 6.5 \times 10^{-18}$ cm^2 and independent of temperature.

Both the reaction kinetics and the *persistent* surface groups could be interpreted in two ways: either two "kinds" of $–CH_3$ exist (e.g., different sites) leading to different reaction paths or the reaction cross section is coverage dependent. Both models could describe the data. The coverage dependent reaction cross sections was determined from the data. From the temperature dependence of the reaction cross section, an activation energy of 0.27 eV was found for the reaction in the H_2O half-cycle. This is comparable to what has been predicted in recent DFT studies (0.25–0.62 eV). In these DFT studies, a coverage dependent reactivity is also reported. Furthermore, in CVD processes, such a coverage dependence is also observed. These facts provide supports for the coverage dependent model, making this the most appropriate model.

The $–CH_3$ coverage was measured with BB-SFG after the TMA and H_2O half-cycles for deposition temperatures between 100 and 450 °C. The trend in the $–CH_3$ coverage after the TMA step showed that the self-limiting behavior in the TMA half-cycle cannot be caused by steric hindrance. The most likely mechanism responsible for the self-limiting nature in the TMA half-cycle is the depletion of under-coordinated O atoms. Furthermore, the $–CH_3$ coverage was quantified in absolute terms and the number of -OH groups consumed in the chemisorption of a TMA molecule on the surface could be determined as a function of temperature. It was found that at 100 °C TMA chemisorbs bifunctionally on the -OH groups with one $–CH_3$ group remaining on the surface after chemisorption. With increasing temperature, this increases to 1.5 $–CH_3$ groups remaining on the surface after TMA chemisorption at 250 °C.

Possible incorporation of the *persistent* $–CH_3$ groups into the Al_2O_3 films was investigated using a dedicated study with XPS. Virtually carbon free films were found when intentionally trying to incorporate $–CH_3$ groups. This result demonstrated that the persistent $–CH_3$ groups are not incorporated in the film and do not necessarily lead to carbon impurities.

Overall, these results demonstrate that BB-SFG spectroscopy can be used to obtain fundamental insight into subtle and intricate elements of the surface chemistry of ALD. The combination of submonolayer sensitivity, inherent surface selectivity, and relatively short acquisition times make BB-SFG spectroscopy ideally suited for mechanistic studies of ALD processes with metal-organic reactants.

ACKNOWLEDGMENTS

The authors would like to thank J. J. A. Zeebregts, J. J. L. M. Meulendijks, C. A. A. van Helvoirt, and C. O. van Bommel for their skillful technical support. This work was

supported by the Dutch Technology Foundation STW and the Netherlands Organization for scientific Research (NWO, VICI Program on "Nanomanufacturing."). W.M.M.K. acknowledges J. W. Coburn and H. F. Winters for the inspiration they provided through their work and for numerous stimulating discussions.

[1]J. W. Coburn and H. F. Winters, J. Vac. Sci. Technol. **16**, 391 (1979).
[2]H. F. Winters and J. W. Coburn, Surf. Sci. Rep. **14**, 162 (1992).
[3]H. F. Winters, J. Vac. Sci. Technol., B **1**, 469 (1983).
[4]F. H. Winters and J. W. Coburn, J. Vac. Sci. Technol., B **3**, 1376 (1985).
[5]H. C. M. Knoops, E. Langereis, M. C. M. van de Sanden, and W. M. M. Kessels, J. Electrochem. Soc. **157**, G241 (2010).
[6]M. D. Groner, F. H. Fabreguette, J. W. Elam, and S. M. George, Chem. Mater. **16**, 639 (2004).
[7]S. E. Potts, W. Keuning, E. Langereis, G. Dingemans, M. C. M. van de Sanden, and W. M. M. Kessels, J. Electrochem. Soc. **157**, P66 (2010).
[8]A. J. M. Mackus, D. Garcia-Alonso, H. C. M. Knoops, A. A. Bol, and W. M. M. Kessels, Chem. Mater. **25**, 1769 (2013).
[9]A. W. Ott, K. C. McCarley, J. W. Klaus, J. D. Way, and S. M. George, Appl. Surf. Sci. **107**, 128 (1996).
[10]M. D. Groner, J. W. Elam, F. H. Fabreguette, and S. M. George, Thin Solid Films **413**, 186 (2002).
[11]G. S. Higashi and C. G. Fleming, Appl. Phys. Lett. **55**, 1963 (1989).
[12]A. C. Dillon, A. W. Ott, J. D. Way, and S. M. George, Surf. Sci. **322**, 230 (1995).
[13]A. W. Ott, J. W. Klaus, J. M. Johnson, and S. M. George, Thin Solid Films **292**, 135 (1997).
[14]R. L. Puurunen, J. Appl. Phys. **97**, 121301 (2005).
[15]V. Miikkulainen, M. Leskelä, M. Ritala, and R. L. Puurunen, J. Appl. Phys. **113**, 021301 (2013).
[16]A. Rahtu, T. Alaranta, and M. Ritala, Langmuir **17**, 6506 (2001).
[17]J. W. Elam, M. D. Groner, and S. M. George, Rev. Sci. Instrum. **73**, 2981 (2002).
[18]V. Vandalon and W. M. M. Kessels, Appl. Phys. Lett. **108**, 011607 (2016).
[19]A. J. M. Mackus, M. J. Weber, N. F. W. Thissen, D. Garcia-Alonso, R. H. J. Vervuurt, S. Assali, A. A. Bol, M. A. Verheijen, and W. M. M. Kessels, Nanotechnology **27**, 034001 (2016).
[20]M. Shirazi and S. D. Elliott, Nanoscale **7**, 6311 (2015).
[21]J. L. van Hemmen, S. B. S. Heil, J. H. Klootwijk, F. Roozeboom, C. J. Hodson, M. C. M. van de Sanden, and W. M. M. Kessels, J. Electrochem. Soc. **154**, G165 (2007).
[22]R. W. Boyd, *Nonlinear Optics*, 2nd ed. (Elsevier Science, Amsterdam, The Netherlands, 1992).
[23]A. B. Voges, H. A. Al-Abadleh, M. J. Musorrafiti, P. A. Bertin, S. T. Nguyen, and F. M. Geiger, J. Phys. Chem. B **108**, 18675 (2004).
[24]V. R. Rai, V. Vandalon, and S. Agarwal, Langmuir **26**, 13732 (2010).
[25]V. R. Rai, V. Vandalon, and S. Agarwal, Langmuir **28**, 350 (2012).
[26]J. Kwon, M. Dai, M. D. Halls, and Y. J. Chabal, Chem. Mater. **20**, 3248 (2008).
[27]E. Langereis, M. Bouman, J. Keijmel, S. B. S. Heil, M. C. M. Van de Sanden, and W. M. M. Kessels, ECS Trans. **16**, 247 (2008).
[28]E. Langereis, J. Keijmel, M. C. M. van de Sanden, and W. M. M. Kessels, Appl. Phys. Lett. **92**, 231904 (2008).
[29]G. Dingemans and W. M. M. Kessels, J. Vac. Sci. Technol., A **30**, 040802 (2012).
[30]R. Matero, A. Rahtu, M. Ritala, M. Leskelä, and T. Sajavaara, Thin Solid Films **368**, 1 (2000).
[31]E. Langereis, S. B. S. Heil, H. C. M. Knoops, W. Keuning, M. C. M. van de Sanden, and W. M. M. Kessels, J. Phys. D: Appl. Phys. **42**, 073001 (2009).
[32]S. E. Potts, G. Dingemans, C. Lachaud, and W. M. M. Kessels, J. Vac. Sci. Technol., A **30**, 021505 (2012).
[33]M. Born and E. Wolf, *Principles of Optics*: *Electromagnetic Theory of Propagation, Interference and Diffraction of Light* (Cambridge University, Cambridge, United Kingdom, 1999).
[34]See supplementary material at http://dx.doi.org/10.1116/1.4993597 for description of the procedure used for calculation of the GPC(at) from the GPC(nm) and original data set.
[35]D. W. Squire, J. Vac. Sci. Technol., B **3**, 1513 (1985).
[36]P. Poodt, J. van Lieshout, A. Illiberi, R. Knaapen, F. Roozeboom, and A. van Asten, J. Vac. Sci. Technol., A **31**, 01A108 (2013).
[37]S. E. Potts and W. M. M. Kessels, Coord. Chem. Rev. **257**, 3254 (2013).
[38]Y. R. Luo and J. A. Kerr, "Bond dissociation energies," in *CRC Handbook of Chemistry and Physics* (CRC, Boca Raton, FL, 2007), pp. 65–98.
[39]E. B. Wilson, J. C. Decius, and P. C. Cross, *Molecular Vibrations* (Dover Publications, New York, 1980).
[40]Q. Du, R. Superfine, E. Freysz, and Y. R. Shen, Phys. Rev. Lett. **70**, 2313 (1993).
[41]P. Miranda, L. Xu, Y. Shen, and M. Salmeron, Phys. Rev. Lett. **81**, 5876 (1998).
[42]A. Boulesbaa and E. Borguet, J. Phys. Chem. Lett. **5**, 528 (2014).
[43]M. Maeda and H. Nakamura, J. Appl. Phys. **55**, 3068 (1984).
[44]M. Bonn, H. Ueba, and M. Wolf, J. Phys.: Condens. Matter **17**, S201 (2005).
[45]I. M. N. Groot, A. W. Kleyn, and L. B. F. Juurlink, J. Phys. Chem. C **117**, 9266 (2013).
[46]S. L. Tait, Z. Dohnálek, C. T. Campbell, and B. D. Kay, J. Chem. Phys. **122**, 164707 (2005).
[47]M. J. P. Hopstaken and J. W. Niemantsverdriet, J. Chem. Phys. **113**, 5457 (2000).
[48]L. A. Okada and S. M. George, Appl. Surf. Sci. **137**, 113 (1999).
[49]T. Weckman and K. Laasonen, Phys. Chem. Chem. Phys. **17**, 17322 (2015).
[50]J. Terry, M. R. Linford, C. Wigren, R. Cao, P. Pianetta, and C. E. D. Chidsey, J. Appl. Phys. **85**, 213 (1999).
[51]A. Fidélis, F. Ozanam, and J. N. Chazalviel, Surf. Sci. **444**, L7 (2000).
[52]G. Dingemans, C. A. A. van Helvoirt, D. Pierreux, W. Keuning, and W. M. M. Kessels, J. Electrochem. Soc. **159**, H277 (2012).
[53]V. Verlaan, L. R. J. G. van den Elzen, G. Dingemans, M. C. M. Van De Sanden, and W. M. M. Kessels, Phys. Status Solidi C **7**, 976 (2010).
[54]S. E. Potts, H. B. Profijt, R. Roelofs, and W. M. M. Kessels, Chem. Vap. Deposition **19**, 125 (2013).